Journal of Alloys and Compounds 509 (2011) 43–51

Contents lists available at ScienceDirect

Journal of Alloys and Compounds

journal homepage: www.elsevier.com/locate/jallcom

Investigation of the Al–Ti–Pd alloy system at 930 and 1100 °C

O.V. Zaikina[a,*], V.G. Khorujaya[a], D. Pavlyuchkov[a,b], B. Grushko[b], T.Ya. Velikanova[a]

[a] Frantsevich Institute for Problems of Materials Science, 03680, Kyiv 142, Ukraine
[b] Institut für Festkörperforschung, Forschungszentrum Jülich, D-52425 Jülich, Germany

ARTICLE INFO

Article history:
Received 28 May 2010
Received in revised form 25 August 2010
Accepted 27 August 2010
Available online 8 September 2010

Keywords:
Phase diagrams
Ternary alloy systems
Laves phases
Titanium aluminides

ABSTRACT

Phase equilibria in the ternary Al–Ti–Pd system have been investigated in the range of the Pd content below 50 at.%. Partial 930 and 1100 °C isothermal sections are constructed.

High-temperature bcc solid solution based on β-Ti (A2) widely extends into ternary compositions. With increasing Pd concentration it obeys the CsCl-type ordering (B2) and this high-temperature ordered solid solution links with that between congruent TiPd and AlPd. The Al-rich end of the low-temperature α-Ti region extends up to 6 at.% Pd. The Al–Ti γ-phase and η-phase extend up to 5 at.% Pd. Other binary Al–Ti and Pd–Ti intermetallics dissolve below 3 at.% of the third element.

Three ternary compounds τ_1, τ_2 and τ_3 reported earlier were confirmed. The τ_1-phase ($Pm\bar{3}m$, $a = 0.39620$ nm) exists in a compositional range between $Al_{60}Ti_{27}Pd_{13}$ and $Al_{70}Ti_{23}Pd_7$ at 1100 °C and between $Al_{61}Ti_{25}Pd_{14}$ and $Al_{69}Ti_{24}Pd_7$ at 930 °C. The τ_2-phase ($Fm\bar{3}m$, $a = 1.22589$ nm) exists between $Al_{53}Ti_{23}Pd_{24}$ and $Al_{54}Ti_{21}Pd_{25}$. The τ_3-phase exists in a range between $Al_{42}Ti_{33}Pd_{25}$ and $Al_{49}Ti_{32}Pd_{19}$ at 1100 °C and between $Al_{40.5}Ti_{33.5}Pd_{26}$ and $Al_{48}Ti_{33}Pd_{19}$ at 930 °C. Apart from the basic structure ($P6_3/mmc$, $a = 0.51383$, $c = 0.82438$ nm) also a superstructure of the of the Nb(Ir,Al)$_2$-type ($P6_3/mcm$, $a = 0.89098(11)$ nm, $c = 0.82011(7)$ nm) was confirmed at the Pd-rich end of this compositional region. According to our preliminary results τ_1 melts incongruently at about 1420 °C while τ_3 melts congruently at 1295 °C. The τ_2-phase is formed in a solid-state reaction between 1050 and 1100 °C.

© 2010 Elsevier B.V. All rights reserved.

1. Introduction

The Al–Ti–Pd alloy system was studied in Ref. [1] at 950 °C in the compositional region below 25 at.% Pd using powder X-ray diffraction and scanning electron microscopy with microprobe compositional analysis. A partial 950 °C isothermal section of Ref. [1] exhibits a wide extension of β-Ti into ternary compositions. At higher Pd and Al concentrations this solid solution was found to have a CsCl-type ordering. The solubility of the third element in the binary Al–Ti and Al–Pd intermetallics was found to be below 2.5 at.%. Three ternary compounds designated τ_1, τ_2 and τ_3 were observed in Ref. [1]. The τ_1-phase of the $AuCu_3$-type was found to be formed around $Al_{61}Ti_{26}Pd_{13}$, τ_2 of the filled Th_6Mn_{23+1}-type around $Al_{52}Ti_{23}Pd_{25}$ and τ_3 of the $MgZn_2$-type Laves structure was found to be formed between $Al_{39.3}Ti_{36.7}Pd_{24}$ and $Al_{48}Ti_{34.3}Pd_{17.7}$. More recently the crystal structures of the τ_1 and τ_2 phases were specified using neutron diffraction [2]. According to Ref. [3], at 950 °C the τ_3-phase exhibits a Nb(Ir,Al)$_2$-type superstructure variant at the Pd-rich end of its compositional region.

In the present work a somewhat wider compositional region of the Al–Pd–Ti phase diagram was studied at 930 °C and a region below 50 at.% Pd at 1100 °C.

2. Experimental

The starting materials were Al of 99.995 mass% purity, Pd of 99.8 mass% and Ti of 99.98 mass%. Ternary alloys (2.5–3 g) of more than 40 compositions were prepared by either arc melting or levitation inductive melting under argon atmosphere. They were subsequently annealed under argon atmosphere at 930 °C for 359–985 h and at 1100 °C for 88–120 h.

The alloys were studied by scanning electron microscopy (SEM), powder X-ray diffraction (XRD). The compositions of the phases were determined in SEM by energy dispersive X-ray analysis (EDX) on polished unetched cross-sections. XRD was carried out in transmission mode using Cu $K_{\alpha 1}$ radiation and an image plate detector (5–120°). Differential thermal analysis (DTA) was carried out for a number of samples at heating and cooling rates of 10–50 K/min.

3. Results and discussion

3.1. Binary terminals

The relevant part of the Al–Pd alloy system contains at the studied temperatures the congruent AlPd phase (β-phase) and the Al_3Pd_2 phase (δ phase) formed by a peritectic reaction $\beta + L \leftrightarrow \delta$ at 952 °C [4]. Their crystallographic data are included in Table 1. Both phases exhibit binary compositional ranges. The Al–Pd system also

* Corresponding author. Tel.: +380 44 424 3090; fax: +380 44 424 2131.
E-mail addresses: alex.zaikina@googlemail.com, alex.zaikina@gmail.com (O.V. Zaikina).

0925-8388/$ – see front matter © 2010 Elsevier B.V. All rights reserved.
doi:10.1016/j.jallcom.2010.08.144

Table 1
Crystallographic data of the Al–Pd–Ti phases in the studied compositional and temperature ranges. The literature data are given with the corresponding references.

Phase	Space group	Prototype	Lattice parameters (nm)		Comment
			a	*c*	
β	$Pm\bar{3}m$	CsCl	0.31406(6)	–	$Al_{30.1}Ti_{38.8}Pd_{31.1}$
			0.31574(7)	–	$Al_{30.1}Ti_{43.3}Pd_{26.6}$
			0.31934(7)	–	$Al_{32.4}Ti_{52.6}Pd_{15.0}$
δ	$P\bar{3}m1$	Al_3Ni_2	0.4227	0.5167	[4]
α	$P6_3/mmc$	Mg	0.29506	0.46835	[6]
α_2	$P6_3/mmc$	Ni_3Sn	0.5775	0.4655	[14]
γ	$P4/mmm$	AuCu	0.4001	0.4071	[14]
η	$I4_1/amd$	$HfGa_2$	0.3976	2.436	[14]
ζ	$P4/mmm$	Ti_2Al_5	0.39053	2.91963	[15]
ζ	$I4/mmm$	$TiAl_3$	0.3846	0.8594	[14]
τ_1	$Pm\bar{3}m$	$AuCu_3$	0.39575	–	$Al_{61}Ti_{26}Pt_{13}$ [1]
			0.39570	–	$Al_{60}Ti_{25}Pt_{15}$ [2]
			0.39620(6)	–	$Al_{62.0}Ti_{25.5}Pd_{12.5}$
			0.39604(11)	–	$Al_{61.2}Ti_{25.6}Pd_{13.2}$
τ_2	$Fm\bar{3}m$	Th_6Mn_{23+1}	1.22295	–	$Al_{52}Ti_{22.8}Pt_{25.2}$ [1]
			1.22379(7)	–	$Al_{52.9}Ti_{22.4}Pd_{24.7}$
τ_3	$P6_3/mmc$	$MgZn_2$	0.51330	0.82603	$Al_{44}Ti_{35}Pt_{21}$ [1]
			0.51383(8)	0.82438(9)	$Al_{45.0}Ti_{32.3}Pd_{22.7}$
			0.51454(9)	0.82446(10)	$Al_{43.5}Ti_{34.1}Pd_{22.4}$
τ_3'	$P6_3/mcm$	$Nb(Ir,Al)_2$	0.89198(3)	0.82040(4)	$Al_{41.0}Ti_{34.5}Pt_{24.5}$ [3]
			0.89098(11)	0.82011(7)	$Al_{44.1}Ti_{29.9}Pd_{26.0}$

contains the so-called ε-phases stable below 792 °C [4], and the γ- and λ-phases formed by solid-state reactions at still lower temperatures. The peritectically solidified ε-phases can be formed in the cast samples as well as the λ-phase forming with (Al) a metastable eutectic [4].

The Ti–Pd phase diagram is accepted in present databases according to Ref. [5]. In the range of 50–100 at.% Ti (see Fig. 1) it exhibited an extended high-temperature solid solution of Pd in bcc β-Ti and a congruent TiPd phase isostructural to the above-mentioned AlPd phase. In the following we use the designation β for the ordered structures and β_{Ti} for the disordered structure. The low-temperature boundary of the β_{Ti} region strongly depends on the composition achieving its maximum of 960 °C at the β_{Ti}-Ti_2Pd phase transition point. This would be important for our 930 °C section, but the compositional range close to Ti–Pd was not studied at this temperature due to sluggish equilibration.

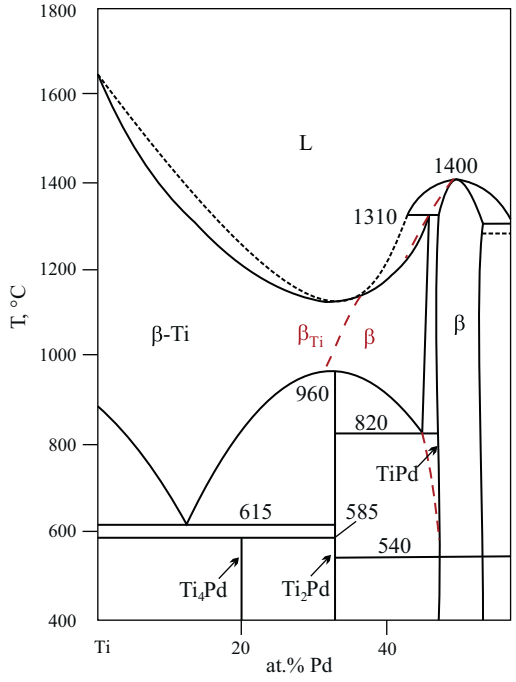

Fig. 1. Ti-rich part of the Ti–Pd phase diagram according to Ref. [5] (solid lines) and according to our suggestion (broken lines, red in the web version of the article).

The Ti–Pd β-phase only differs from the β_{Ti}-phase by a CsCl-type ordering (i.e. B2 vs. A2 structures). This could imply the second-order transition between the phases rather than the first-order transition, as in the diagram of Ref. [5], and a continuity of their compositional regions. Indeed, such a continuity was revealed in Al–Fe [6] or Ti–Rh [7] or Al–Ti (see below). In contrast, in the diagram of Ref. [5] the ranges of the ordered and disordered bcc phases are separated by a narrow two-phase region. However, this was not observed directly in this study: all the samples in the range of 0–52 at.% Pd quenched from 1000 °C are shown to be single-phase. Their structures forming at the annealing temperature could not be concluded from either metallography or room-temperature diffraction examinations due to the very rapid transformation of the high-temperature phase(s) by cooling. The existence of the two-phase region was probably concluded on the basis of thermal analysis experiments, interpreted as evidence of the isothermal transitions at 820 and 1310 °C (Fig. 1). In our DTA experiments no transition at 820 °C was observed supporting a suggestion of the compositional continuity of β and β_{Ti}. For technical reason the samples were not studied in our work up to their melting, while the results at 1310 °C mentioned in Ref. [5] can also be interpreted in favor of one continuous region. This casts doubt on the correctness of this item in the generally accepted Ti–Pd phase diagram.

Moreover, it is plausible that the boundary between the A2 and B2 structures lies at higher Ti concentrations and the boundary shifts towards higher Ti with decreasing temperature (broken line in Fig. 1). Diffusion-couple experiments in Ref. [8] did not reveal any discontinuity in the range from pure Ti to 50 at.% Pd. Instead, the concentration profile obtained in this work at 1000 °C exhibited a singularity at ~30 at.% Pd, which was suggested by these authors to correspond to the A2/B2 boundary. Actually, the ordering could be a reason for the increase in the melting temperature of the solid solution, while the dissolution of Pd in the disordered phase results in its decrease. The suggested constitution of Ti–Pd is also supported by an examination of ternary alloys (see below), which also did not exhibit any two-phase region between the regions extended from β-Ti and β-TiPd. In contrast to binary Ti–Pd β-phase, that in the studied ternary alloys could be quenched and examined by room temperature XRD. The corresponding lattice parameters of β in several studied samples are included in Table 1.

Table 2
Powder XRD data of the τ_1-phase of the $Al_{62.0}Ti_{25.5}Pd_{12.5}$ composition ($Pm\bar{3}m$, $a = 0.39620(6)$ nm, $V = 0.062194(17)$ nm^3).

No.	h	k	l	d_{obs}	d_{calc}	I/I_{0obs}
1	1	1	1	0.22873	0.22875	100
2	2	0	0	0.19814	0.19810	47
3	2	2	0	0.14005	0.14008	19
4	3	1	1	0.11949	0.11946	18
5	2	2	2	0.11436	0.11437	5
6	4	0	0	0.09905	0.09905	2

The Al–Ti alloy system has been very extensively studied but a complete agreement has not yet been achieved. In Ref. [9] the two most recent versions of Al–Ti published in Refs. [10,11] are presented and discussed. In the temperature range relevant to our study both diagrams in Refs. [10,11] are consistent. Thus, at 1100 °C the system contains (see Table 1 for crystallographic data) β_{Ti} extending up to ~20 at.% Al, α, $\alpha_2(AlTi_3)$, γ(AlTi), η(Al_2Ti), ζ(Al_5Ti_2) and high-temperature € (Al_3Ti). The controversies were mainly revealed at higher temperatures. However, the dissolution of Pd in binary Al–Ti phases is expected to reduce the transition temperatures, as is observed in other Al–Pd–TM alloy systems (see [12] for references). Therefore it is worth mentioning two relevant items:

- the A2 ↔ B2 order–disorder transition in β-Ti is accepted in [10], but the ordering is missing in [11];
- the ranges of γ and ζ are separated in [10] by a narrow two-phase region and are associated with separate phases, while in [11] they are linked above 1215 °C in a continuous range, where the high-Al part is associated with a one-dimensional anti-phase structure (1D-APS).

The propagation of the binary phases into the ternary space is presented in Section 3.3.

Concerning the Al–Pd ε-phases forming below the studied temperatures and observed in solidified liquid phase, their maximal Ti concentration was in the order of 0.5 at.%. This observation is consistent with the previous results, which point to a decrease of this value from 16 at.% of Ni or Co via 10 at.% of Fe and 5 at.% of Mn [12] to 3 at.% for Cr [13].

3.2. Ternary phases

Three ternary phases reported earlier in Ref. [1] were confirmed in our study. In the following we use their same designations as in [1] (see Table 1). The powder X-ray diffraction data of the ternary phases are given in Tables 2–4. We also confirm the existence of the $Nb(Ir,Al)_2$-type superstructure at the Pd-rich end of the τ_3 compositional region reported recently in Ref. [3] (see Table 1). The corresponding XRD data of the almost single-phase sample $Al_{44.0}Ti_{30.8}Pt_{25.2}$ are presented in Table 5. In Section 3.3 only one τ_3-region is shown, since we could not find any splitting of the region associated with two types of structures.

According to our preliminary results τ_1 melts incongruently at about 1420 °C while τ_3 melts congruently at 1295 °C. The transformation temperature of the τ_2-phase was only estimated to be between 1050 and 1100 °C. Indeed, DTA examinations of the samples containing this essentially single-phase (an $Al_{52}Ti_{23}Pd_{25}$ alloy annealed at 930 °C) indicated by heating at 20 K/min a weak endothermic effect starting at 1126 °C and a strong endothermic effect starting at 1165 °C (Fig. 2a). The former could be associated with a solid-state transformation of the τ_2-phase and the latter with the eutectic reaction $L \leftrightarrow \tau_1 + \tau_3 + \beta$. On the other hand, the above-mentioned $Al_{52}Ti_{23}Pd_{25}$ alloy annealed at 1100 °C exhibited the $\tau_1 + \tau_3 + \beta$ equilibrium, which contradicts the existence of the τ_2-phase at the annealing temperature. In order to clarify

Table 3
Powder XRD data of the τ_2-phase of the $Al_{52.9}Ti_{22.4}Pd_{24.7}$ composition ($Fm\bar{3}m$, $a = 1.22379(7)$ nm, $V = 1.83283(19)$ nm^3).

No.	h	k	l	d_{obs}	d_{calc}	I/I_{0obs}
1	1	1	1	0.70746	0.70656	2
2	2	0	0	0.61281	0.61190	1
3	2	2	0	0.43285	0.43268	6
4	3	1	1	0.36841	0.36899	2
5	2	2	2	0.35300	0.35328	36
6	4	0	0	0.30573	0.30595	33
7	3	3	1	0.28062	0.28076	3
8	4	2	2	0.24979	0.24981	10
9	5	1	1	0.23537	0.23552	13
10	4	4	0	0.21624	0.21634	100
11	5	3	1	0.20689	0.20686	4
12	6	0	0	0.20401	0.20397	3
13	6	2	0	0.19347	0.19350	3
14	6	2	2	0.18452	0.18449	23
15	4	4	4	0.17663	0.17664	7
16	6	4	2	0.16357	0.16354	1
17	7	3	1	0.15937	0.15932	4
18	8	0	0	0.15298	0.15297	9
19	7	3	3	0.14948	0.14951	1
20	6	6	0	0.14423	0.14423	3
21	7	5	1	0.14134	0.14131	1
22	6	6	2	0.14041	0.14038	7
23	8	4	0	0.13681	0.13682	8
24	9	1	1	0.13433	0.13433	2
25	8	4	2	0.13355	0.13353	2
26	6	6	4	0.13047	0.13046	1
27	9	3	1	0.12830	0.12829	2
28	8	4	4	0.12492	0.12490	14
29	7	7	1	0.12300	0.12300	2
30	10	2	0	0.12000	0.12000	1
31	9	5	1	0.11831	0.11831	3
32	10	2	2	0.11778	0.11776	6
33	8	8	0	0.10817	0.10817	4
34	10	6	2	0.10344	0.10343	7
35	12	0	0	0.10199	0.10198	2
36	12	4	0	0.09674	0.09675	3
37	10	6	6	0.09329	0.09331	1
38	12	4	4	0.09224	0.09225	1
39	13	3	1	0.09148	0.09147	1

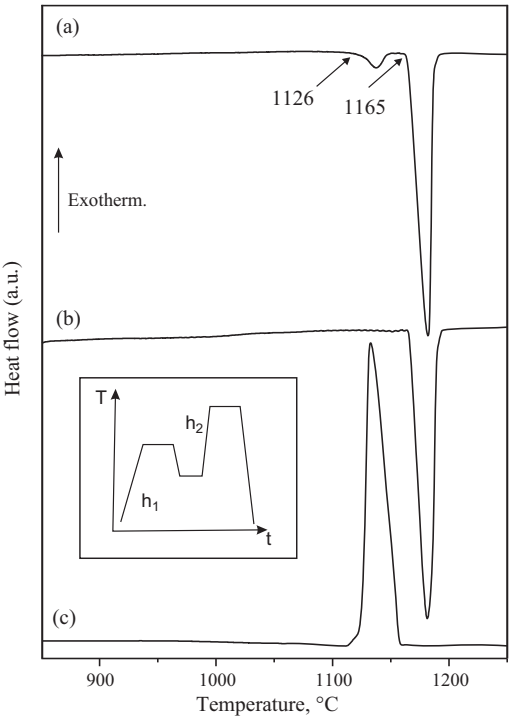

Fig. 2. DTA plots of the $Al_{52}Ti_{23}Pd_{25}$ alloy annealed at 930 °C: (a) heating branch (20 K/min), (b) as (a) after preannealing at 1100 °C, and (c) cooling branch (50 K/min).

Table 4
Powder XRD data of the τ_3-phase of the $Al_{45.0}Ti_{32.3}Pd_{22.7}$ composition ($P6_3/mmc$, $a = 0.51383(8)$ nm, $c = 0.82438(9)$ nm, $V = 0.18850(4)$ nm^3).

No.	h	k	l	d_{obs}	d_{calc}	I/I_{0obs}
1	1	0	0	0.44492	0.44499	11
2	0	0	2	0.41223	0.41219	4
3	1	0	1	0.39201	0.39159	6
4	1	1	0	0.25660	0.25692	28
5	1	0	3	0.23373	0.23381	70
6	2	0	0	0.22239	0.22250	12
7	1	1	2	0.21810	0.21803	100
8	2	0	1	0.21496	0.21481	75
9	0	0	4	0.20619	0.20609	22
10	2	0	2	0.19583	0.19579	31
11	1	0	4	0.18713	0.18701	16
12	2	0	3	0.17289	0.17292	7
13	2	1	0	0.16812	0.16819	5
14	3	0	0	0.14829	0.14833	4
15	2	1	3	0.14338	0.14345	18
16	3	0	2	0.13953	0.13957	21
17	0	0	6	0.13736	0.13740	3
18	2	0	5	0.13250	0.13247	21
19	1	0	6	0.13132	0.13128	4
20	2	1	4	0.13038	0.13031	11
21	2	2	0	0.12853	0.12846	20
22	2	0	6	0.11693	0.11690	13
23	3	1	3	0.11258	0.11258	10
24	3	0	5	0.11026	0.11027	8
25	2	2	4	0.10901	0.10902	11
26	4	0	2	0.10741	0.10740	2
27	3	1	4	0.10590	0.10588	4
28	2	0	7	0.10405	0.10409	4
29	0	0	8	0.10307	0.10305	3
30	1	0	8	0.10036	0.10039	4

this contradiction, additional DTA were carried out according to the following procedure (see inset in Fig. 2). The samples, initially annealed at 930 °C and containing essentially single τ_2-phase, were heated up to either 1050 or 1100 °C, kept for one hour at the set temperature, cooled to 700 °C and then heated at 20 K/min to 1250 °C. In the case of the 1-h annealing at 1050 °C the above-mentioned effect at 1126 °C was observed, but it was missing after the annealing at 1100 °C (Fig. 2b). This indicated the decomposition of the τ_2-phase between 1050 and 1100 °C and a strong superheating of the τ_2-phase in the DTA experiments.

At 1100 °C the τ_1-phase exists in the compositional region between $Al_{60}Ti_{27}Pd_{13}$ and $Al_{70}Ti_{23}Pd_7$, and at 930 °C between $Al_{61}Ti_{25}Pd_{14}$ and $Al_{69}Ti_{24}Pd_7$. The homogeneity regions of the τ_3-phase are between $Al_{42}Ti_{33}Pd_{25}$ and $Al_{49}Ti_{32}Pd_{19}$ at 1100 °C, between $Al_{40.5}Ti_{33.5}Pd_{26}$ and $Al_{48}Ti_{33}Pd_{19}$ at 930 °C. The τ_2-phase exists in a narrow concentration region between $Al_{53}Ti_{23}Pd_{24}$ and $Al_{54}Ti_{21}Pd_{25}$.

3.3. Isothermal sections

At 1100 °C the isothermal section was studied in the compositional range below 50 at.% Pd (Fig. 3, Table 6). The section between the congruent AlPd and TiPd naturally separates this range from the high-Pd part of the phase diagram. These isostructural phases form a continuous range of the β solid solutions. Accepting the continuity of the ordered and disordered bcc ranges in PdTi, their total range can be drawn propagating up to the limits of this phase in Al–Ti. The boundary between the ordered and disordered β surrounding the Ti corner was not detected. Indeed, in all relevant studied samples the B2 structure was revealed, but none of the samples was studied close to the Ti-rich part of the binary Ti–Pd system.

The solubility of Pd in Al–Ti intermetallics is quite low. The propagation of α (up to 6 at.% Pd) was only measured in a single sample. The solubility of Pd in α_2 was up to 2 at.%. In the compositional

Table 5
Powder XRD data of the τ_3'-phase of the $Al_{44.1}Ti_{29.9}Pd_{26.0}$ composition ($P6_3/mcm$, $a = 0.89098(11)$ nm, $c = 0.82011(7)$ nm, $V = 0.56381(12)$ nm^3).

No.	h	k	l	d_{obs}	d_{calc}	I/I_{0obs}
1	1	1	0	0.44641	0.44549	19
2	0	0	2	0.41015	0.41005	2
3	1	1	1	0.39145	0.39146	5
4	2	0	0	0.38550	0.38580	2
5	1	0	2	0.36225	0.36210	18
6	1	1	2	0.30184	0.30170	3
7	2	1	0	0.29165	0.29164	4
8	2	0	2	0.28099	0.28099	1
9	2	1	1	0.27487	0.27478	4
10	3	0	0	0.25723	0.25720	32
11	1	1	3	0.23297	0.23300	63
12	2	2	0	0.22275	0.22274	7
13	3	0	2	0.21784	0.21789	100
14	2	2	1	0.21502	0.21496	86
15	0	0	4	0.20501	0.20503	22
16	2	1	3	0.19942	0.19945	2
17	2	2	2	0.19576	0.19573	24
18	1	1	4	0.18628	0.18625	16
19	2	0	4	0.18095	0.18105	1
20	3	2	0	0.17691	0.17702	1
21	4	0	2	0.17448	0.17455	1
22	2	2	3	0.17267	0.17268	5
23	4	1	0	0.16841	0.16838	6
24	2	1	4	0.16771	0.16773	2
25	3	3	0	0.14852	0.14850	4
26	3	3	1	0.14614	0.14612	1
27	5	0	2	0.14437	0.14443	1
28	4	1	3	0.14342	0.14337	13
29	3	3	2	0.13964	0.13962	17
30	4	2	2	0.13745	0.13739	1
31	0	0	6	0.13669	0.13668	3
32	1	0	6	0.13459	0.13459	1
33	3	2	4	0.13412	0.13399	1
34	2	2	5	0.13211	0.13208	19
35	1	1	6	0.13064	0.13067	5
36	3	1	5	0.13016	0.13018	10
37	4	2	3	0.12864	0.12866	16
38	5	2	0	0.12353	0.12356	1
39	3	0	6	0.12072	0.12070	1
40	6	1	0	0.11761	0.11767	1
41	2	2	6	0.11652	0.11650	8
42	1	1	7	0.11325	0.11331	1
43	5	2	3	0.11262	0.11259	6
44	4	4	0	0.11142	0.11137	1
45	4	4	1	0.11038	0.11036	5
46	4	2	5	0.10897	0.10898	7
47	4	3	4	0.10785	0.10787	1
48	4	4	2	0.10752	0.10748	2
49	6	2	1	0.10609	0.10610	2
50	5	2	4	0.10584	0.10583	2
51	2	2	7	0.10370	0.10369	2
52	4	4	3	0.10313	0.10314	1
53	0	0	8	0.10245	0.10251	1
54	7	1	1	0.10142	0.10142	1
55	3	3	6	0.10055	0.10057	1
56	1	1	8	0.09990	0.09990	2
57	7	1	2	0.09919	0.09917	1
58	6	3	0	0.09721	0.09721	1
59	4	1	7	0.09614	0.09617	1
60	7	1	3	0.09573	0.09573	3
61	3	0	8	0.09523	0.09523	1
62	6	2	4	0.09478	0.09486	1
63	6	3	2	0.09459	0.09459	5
64	6	0	6	0.09367	0.09366	2
65	4	4	5	0.09214	0.09214	2
66	7	2	2	0.09188	0.09187	1
67	5	2	6	0.09165	0.09166	1
68	1	1	9	0.08929	0.08927	1
69	7	2	3	0.08911	0.08912	1
70	4	1	8	0.08758	0.08756	2
71	2	1	9	0.08699	0.08698	1
72	4	4	6	0.08636	0.08634	2

Table 6
Composition of phases observed in alloys annealed at 1100 °C.

No.	Alloy composition (at.%)			Annealing time (h)	Phase	Phase composition (at.%)		
	Al	Ti	Pd			Al	Ti	Pd
1	17.4	63.2	19.4	88	β	17.4	63.0	19.6
2	26.8	69.2	4.0	236	α_2	27.2	70.6	2.2
					α-Ti	25.1	68.8	6.1
3	23.1	42.4	34.5	68	β	23.8	42.7	33.5
4	28.6	50.9	20.5	95	β	27.8	52.8	19.4
5	30.0	38.9	31.1	88	β	30.1	38.8	31.1
6	29.5	40.8	29.7	114	β	30.4	40.5	29.2
7	30.2	43.3	26.5	88	β	30.1	43.3	26.6
8	32.4	52.6	15.0	88	β	32.4	52.6	15.0
9	33.8	51.4	14.8	114	β	36.2	48.9	14.9
10	35.0	53.8	11.2	93	β	36.6	51.6	11.8
11	35.3	28.8	35.9	114	β	35.2	28.9	35.9
12	36.8	44.2	19.0	88	τ_3	42.2	34.4	23.4
					β	36.4	44.8	18.8
13	37.2	49.3	13.5	114	β	37.3	49.2	13.5
14	37.8	47.3	14.9	93	β	37.9	47.2	14.9
15	39.1	55.1	5.8	119	α_2	38.8	58.5	2.7
					β	38.7	55.2	6.1
16	40.6	29.2	30.2	96	τ_3	42.5	32.6	24.9
					β	38.4	24.4	37.2
17	41.2	36.5	22.3	88	τ_3	42.8	33.7	23.5
					β	36.9	45.3	17.8
18	43.8	50.8	5.4	88	γ	47.2	49.1	3.7
					β	40.1	51.9	8.0
19	44.1	40.5	15.4	119	τ_3	45.5	34.0	20.5
					β	40.1	48.6	11.3
					γ	47.6	48.3	4.1
20	45.1	32.2	22.7	88	τ_3	45.0	32.3	22.7
21	44.0	24.2	31.8	114	τ_3	44.2	32.7	23.1
					β	46.6	5.1	48.3
22	46.2	35.7	18.1	68	γ	48.1	47.8	4.1
					τ_3	45.9	33.5	20.6
23	47.9	40.2	11.9	95	γ	50.5	46.5	3.0
					τ_3	46.9	33.8	19.3
24	49.5	45.1	5.4	68	γ	50.1	46.4	3.5
					τ_3	47.4	33.5	19.1
25	50.0	30.7	19.3	88	τ_1	61.6	24.9	13.5
					τ_3	48.7	31.7	19.6
					β	49.4	2.7	47.9
26	52.6	23.3	24.1	88	τ_1	61.7	25.1	13.2
					τ_3	48.9	31.8	19.3
					β	49.4	2.7	47.9
27	53.2	40.9	5.9	68	γ	54.5	42.1	3.4
					τ_3	49.0	32.7	18.3
					τ_1[a]	58.0	29.9	12.1
28	53.5	18.1	28.4	88	τ_1	61.2	25.1	13.7
					τ_3	48.6	31.8	19.6
					β	49.9	1.7	48.4
29	58.3	36.6	5.1	68	γ	56.7	40.8	2.5
					τ_1	61.9	28.5	9.6
30	57.6	36.7	5.7	95	γ	55.7	41.4	2.9
					τ_1	60.6	28.7	10.7
31	62.2	25.3	12.5	95	τ_1	62.0	25.5	12.5
32	60.3	34.1	5.6	164	γ	58.6	39.2	2.2
					τ_1	63.3	27.8	8.9
33	62.7	32.0	5.3	164	γ	60.8	37.1	2.1
					τ_1	63.8	28.1	8.1
34	63.0	30.7	6.3	95	η	64.9	32.2	2.9
					τ_1	64.8	27.9	7.3
35	62.4	19.1	18.5	209	τ_1	65.6	24.6	9.8
					β	53.6	0.6	45.8
36	66.2	27.8	6.0	202	τ_1	66.2	26.7	7.1
					η	66.6	30.0	3.4
37	69.1	25.6	5.3	164	ζ	71.3	27.6	1.1
					τ_1	68.2	25.7	6.1
38	69.4	23.9	6.7	88	ε	75.2	24.4	0.4
					τ_1	69.7	23.6	6.7
					L	71.2	0.8	28.0
39	73.8	18.8	7.4	88	ε	75.1	24.4	0.5
					τ_1	70.0	23.4	6.6
					L	71.2	0.5	28.3

[a] Small amount of the phase.

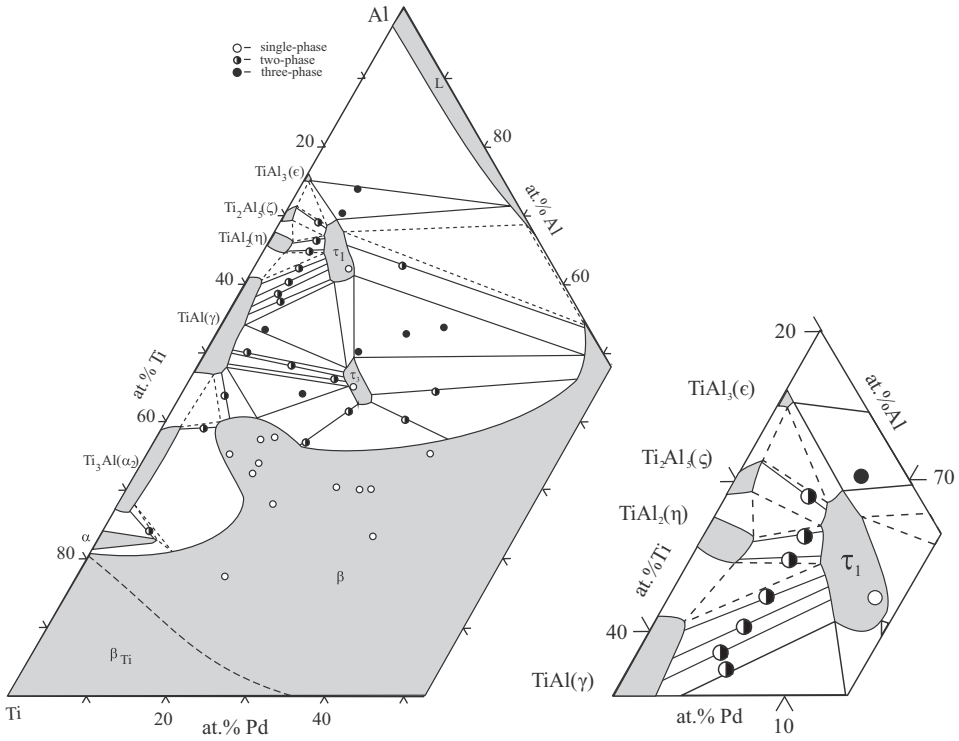

Fig. 3. Partial 1100 °C isothermal section. In the inset: enlarged part of the diagram adjacent to the regions of γ and η. The liquid is designated L. The compositions of the studied samples are shown by spots. Provisional tie-lines are shown by broken lines.

range adjacent to those of the Al–Ti γ and η phases our experiments only revealed two-phase equilibria between one of the binaries and ternary τ_1 (see Fig. 3). The γ and η phases have similar structures and the expected powder XRD patterns of η should contain weak reflections in addition to those of the γ-phase (see Ref. [14]). The corresponding powder XRD patterns only exhibited a basic structure typical of the γ-phase, while additional reflections could be at the level of the instrumental noise. On the other hand, examinations of these alloys at 930 °C (see below) revealed quite similar ternary extensions of γ and η and a three-phase equilibrium of these phases with τ_1. Based on these observations we assume a similar $\tau_1 + \gamma + \eta$ equilibrium at 1100 °C.

The τ_1- and τ_3-phases exhibited visible compositional regions. The τ_2-phase does not exist in the 1100 °C section. The three-phase equilibria $\tau_1 + \tau_3 + \beta$, $\beta + \gamma + \tau_3$, $\tau_1 + \tau_3 + \gamma$ and $\tau_1 + \epsilon + L$ were established directly. The $\beta + \alpha + \alpha_2$, $\beta + \alpha_2 + \gamma$, $\tau_1 + \zeta + \eta$, $\tau_1 + \zeta + \epsilon$ and $\tau_1 + \beta + L$ equilibria were concluded on the basis of the investigation of two-phase and neighboring three-phase samples.

In order to be not very close to the temperature of the $\beta + L \leftrightarrow \delta$ reaction (952 °C) we investigated the ternary phase diagram at 930 °C and not at 950 °C as in Ref. [1]. At 930 °C the studied compositional region was smaller (Fig. 4, Table 7). The Al–Pd δ-phase is stable at this temperature. In Al–Ti the same phases as at 1100 °C are stable, apart from the ζ-phase, which decomposes into η and ϵ already at 976 °C. All three ternary phases are formed. The τ_1-phase was found in a three-phase equilibrium with two binaries, identified with γ and η according to their compositions. The Pd concentration in η was 4 at.%, which is in favor of a stronger propagation of this phase also at higher temperatures, i.e. the existence of a similar three-phase equilibrium at 1100 °C as was suggested above. The three-phase equilibria $\tau_1 + \tau_2 + \beta$, $\tau_2 + \tau_3 + \beta$, $\tau_1 + \tau_2 + \tau_3$ and $\beta + \gamma + \tau_3$, $\tau_1 + \tau_3 + \gamma$, $\tau_1 + \gamma + \eta$, $\beta + \delta + \tau_1$, $\epsilon + \delta + L$ were established directly, while $\tau_1 + \eta + \epsilon$ and $\tau_1 + \delta + \epsilon$ were concluded on the basis of the investigation of two-phase samples.

As compared to the results in Ref. [1], our study at very similar temperature (930 °C vs. 950 °C) revealed somewhat different concentration regions of ternary phases and ternary extensions of binaries (see Fig. 5). Apart from this, the $\alpha_2 + \tau_3$ equilibrium reported in Ref. [1] is not possible together with the $\beta + \gamma$ equilibrium observed in our experiments (see Fig. 5). The latter was confirmed by investigation of a series of relevant samples (see

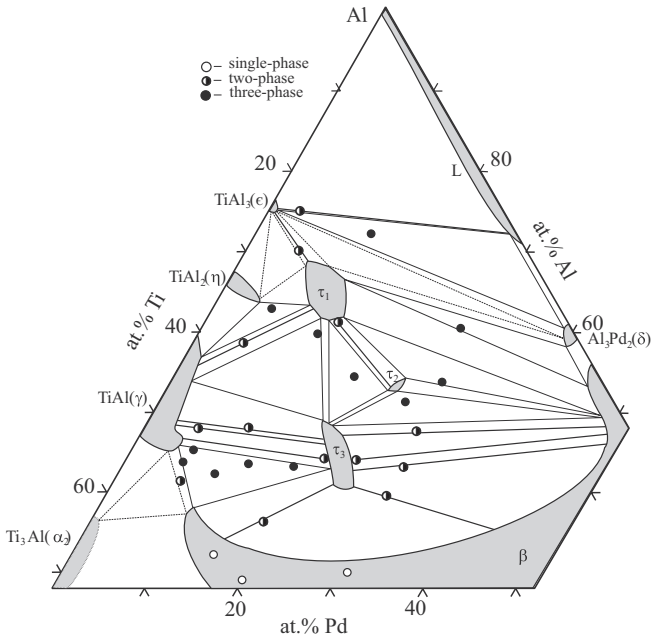

Fig. 4. Partial 930 °C isothermal section. The liquid is designated L. The compositions of the studied samples are shown by spots. Provisional tie-lines are shown by broken lines.

Table 7
Composition of phases observed in alloys annealed at 930 °C.

No.	Alloy composition (at.%)			Annealing time (h)	Phase	Phase composition (at.%)		
	Al	Ti	Pd			Al	Ti	Pd
1	28.3	51.1	20.6	985	β	28.9	51.3	19.8
2	30.7	38.1	31.2	1267	β	29.9	37.5	32.6
3	32.2	51.9	15.9	1267	β	32.5	51.9	15.6
4	36.3	45.1	18.6	985	τ_3	40.9	34.9	24.2
					β	34.1	50.4	15.5
5	39.2	30.0	30.8	1267	τ_3	40.5	33.5	26.0
					β	35.5	21.1	43.4
6	41.8	50.8	7.4	400	β	38.6	51.1	10.3
					γ	47.3	47.8	4.9
7	42.4	47.0	10.6	400	β	38.5	50.8	10.7
					γ	46.7	47.6	5.7
					τ_3	44.9	32.7	22.4
8	43.7	50.7	5.6	1267	γ	45.8	49.6	4.6
					β	37.1	52.5	10.4
					τ_3	43.2	34.9	21.9
9	43.2	25.8	31.0	985	τ_3	42.4	32.9	24.7
					β	46.6	2.6	50.8
10	43.3	37.7	19	400	β	38.4	50.9	10.7
					γ	47.3	46.8	5.9
					τ_3	44.4	32.0	23.6
11	43.8	42.3	13.9	400	β	38.9	49.9	11.2
					γ	47.6	47.1	5.3
					τ_3	44.6	32.9	22.5
12	44.0	30.8	25.2	400	τ_3	44.5	30.4	25.1
					β[a]	47.0	7.3	45.7
13	44.0	33.4	22.6	1267	τ_3	43.5	34.1	22.4
					γ	46.8	48.0	5.2
14	46.9	46.6	6.5	400	β	38.8	50.3	10.9
					γ	46.6	47.9	5.5
					τ_3	44.6	34.0	21.4
15	48.1	40.8	11.1	985	γ	48.9	48.1	3.0
					τ_3	46.4	33.0	20.6
16	47.8	46.3	5.9	985	γ	48.7	47.9	3.4
					τ_3	45.8	33.1	21.1
17	47.0	23.1	29.9	1267	τ_3	47.0	31.0	22.0
					β	48.5	0.9	50.6
18	50.8	22.8	26.4	985	τ_3	48.0	32.3	19.7
					τ_2	52.9	22.4	24.7
					β	49.5	2.2	48.3
19	53.4	17.5	29.1	985	τ_1	61.6	23.4	15.0
					τ_2	54.2	20.8	25.0
					β	49.3	2.2	48.5
20	55.0	25.5	19.5	985	τ_1	61.5	25.3	13.2
					τ_3	48.5	32.0	19.5
					τ_2	52.7	22.8	24.5
21	58.4	35.9	5.7	68	γ	55.9	42.2	1.9
					τ_1	63.1	26.0	10.9
22	60.0	26.5	13.5	985	τ_1	61.4	26.1	12.5
					τ_3	49.9	31.9	18.2
					γ*	58.5	33.8	7.7
23	60.4	11.6	28.0	358	τ_1	66.8	21.6	11.6
					β	53.4	0.7	45.9
					δ	55.7	3.5	40.7
24	61.6	24.6	13.8	985	τ_1	61.2	25.6	13.2
					τ_2	52.7	23.4	23.9
25	63.0	30.6	6.4	985	γ	56.4	41.9	1.7
					η	63.8	30.3	5.9
					τ_1	63.5	25.7	10.8
26	70.2	24.1	5.7	358	τ_1	68.9	23.3	7.8
					ε	75.6	24.0	0.4
27	72.3	15.0	12.7	358	ε	75.5	24.2	0.3
					δ	59.4	0.5	40.1
					L	71.9	0.8	27.4
28	74.6	22.2	3.2	358	ε	75.3	24.2	0.5
					L	71.6	0.4	28.0

[a] Small amount of the phase.

Table 7). For example, a powder XRD pattern presented in Fig. 6 corresponding to a two-phase structure of $Al_{41.8}Ti_{50.8}Pd_{7.4}$ depicted in Fig. 7 shows the coexistence of the β and γ phases. The same β + γ equilibrium was also observed at 1100 °C confirming that the differences between our work and Ref. [1] are not due to a small differences in annealing temperatures. Additionally, in our DTA experiment with the above-mentioned $Al_{41.8}Ti_{50.8}Pd_{7.4}$, a thermal effect corresponding to a phase transition was revealed at ~780 °C,

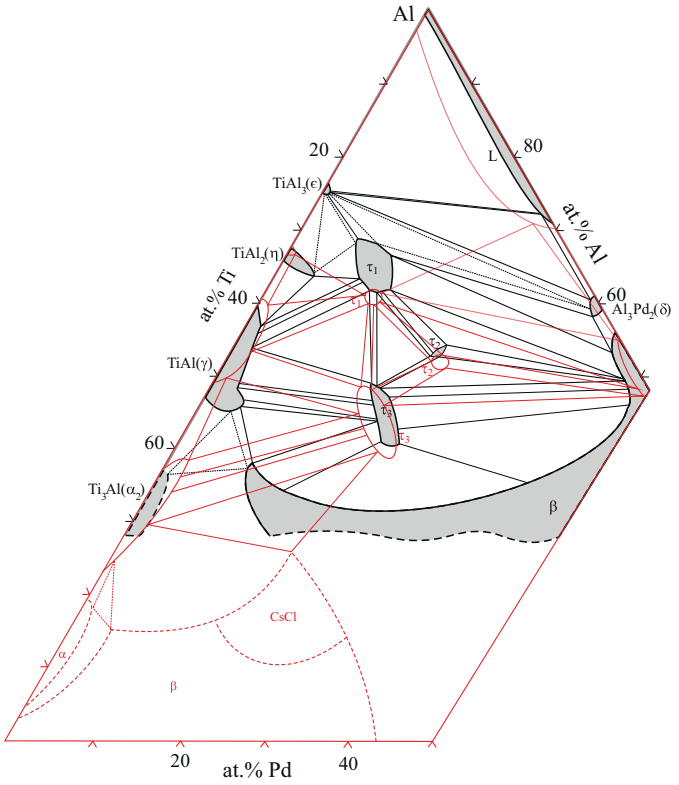

Fig. 5. The results of the present study as in Fig. 4 compared to those in Ref. [1] obtained for 950 °C (thin lines, red in the online version).

i.e. much below our annealing temperatures, but no any other thermal effects occurred in this material up to our upper annealing temperature (1100 °C, see Fig. 8). Therefore the $\alpha_2 + \tau_3$ equilibrium reported in Ref. [1] could in fact be at somewhat lower temperatures.

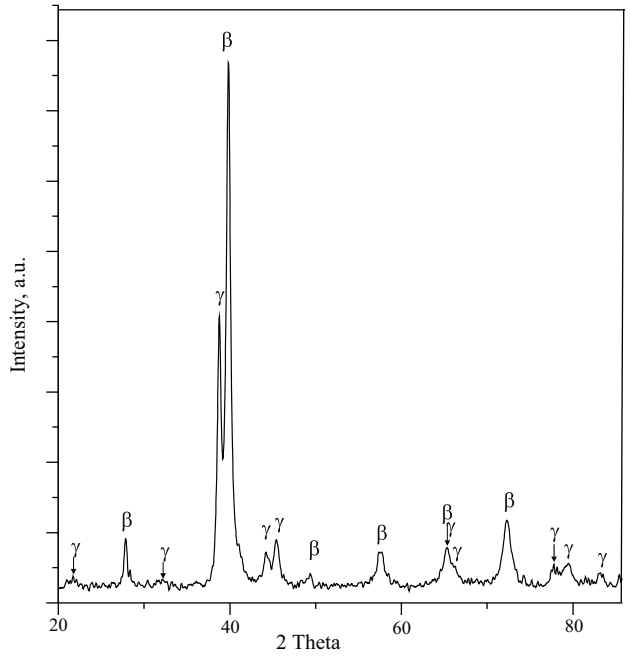

Fig. 6. Powder XRD pattern (Cu $K_{\alpha 1}$ radiation) of the $Al_{41.8}Ti_{50.8}Pd_{7.4}$ alloy annealed at 930 °C for 400 h.

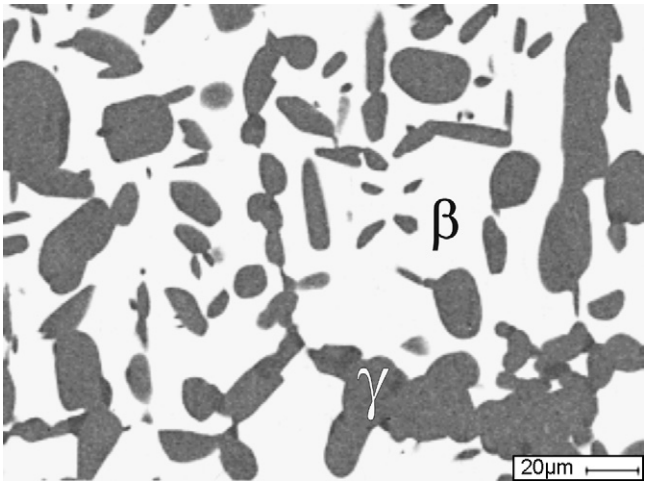

Fig. 7. Backscattered electron image of the $Al_{41.8}Ti_{50.8}Pd_{7.4}$ alloy annealed at 930 °C for 400 h. (Bright is the β-phase of the $Al_{38.6}Ti_{51.1}Pd_{10.3}$ of composition, dark is the γ-phase of the $Al_{47.4}Ti_{47.7}Pd_{4.9}$ of composition.)

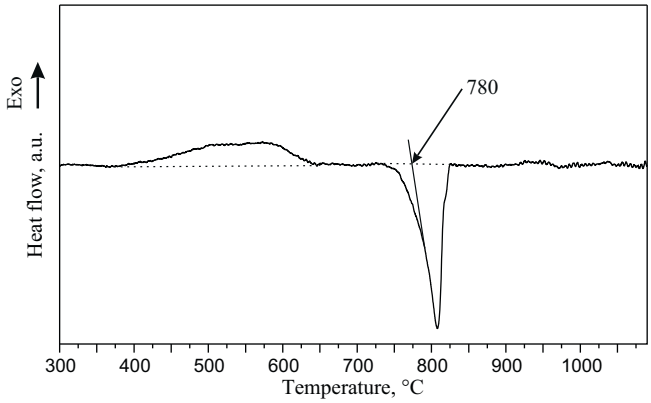

Fig. 8. DTA plot of the $Al_{41.8}Ti_{50.8}Pd_{7.4}$ alloy annealed at 930 °C for 400 h (heating branch, 20 K/min).

4. Summary

Partial 930 and 1100 °C isothermal sections of the Al–Ti–Pd phase diagram were determined. The CsCl-type β solid solution is formed between TiPd and AlPd and widely extends towards Al–Ti. The second-order transition between the β_{Ti} and β phase presumably exists quite close to the Ti corner. The Al-rich end of the low-temperature α-Ti region extends up to 6 at.% Pd. The Al–Ti γ-phase and η-phase extend up to 5 at.% Pd. Other binary Al–Ti and Pd–Ti intermetallics dissolve below 3 at.% of the third element. Three ternary compounds: τ_1 (of $AuCu_3$-type), τ_2 (of Th_6Mn_{23+1}-type) and τ_3 (of $MgZn_2$-type) reported earlier in Refs. [1,2] were confirmed. Additionally, the existence of the τ_3' phase with the $Nb(Ir,Al)_2$-type structure was confirmed in the compositional range similar to that early determined in Ref. [3]. Only the τ_1 and τ_3-phases were found to be stable at 1100 °C, while the τ_2-phase is formed in the solid state between 1050 and 1100 °C. The existence of the $\tau_1 + \tau_3 + \beta$ equilibrium at 1100 °C and the $\tau_1 + \tau_2 + \beta$, $\tau_2 + \tau_3 + \beta$, $\tau_1 + \tau_2 + \tau_3$ equilibria at 930 °C indicates a peritectoid character of the τ_2-phase formation.

Acknowledgements

We thank M. Schmidt, V. Lenzen, A. Besmehn and B. Jülich for technical contributions. A.Z. and T.V. thank Forschungszentrum Jülich for hospitality.

References

[1] J.J. Ding, P. Rogl, B. Chevalier, J. Etourneau, Intermetallics 8 (2000) 1377.
[2] A. Grytsiv, P. Rogl, H. Schmidt, G. Giester, P. Hundegger, G. Wiesinger, V. Pomjakushin, Intermetallics 12 (2004) 563.
[3] X. Yan, A. Grytsiv, P. Rogl, H. Schmidt, G. Giester, A. Saccone, X.-Q. Chen, Intermetallics 17 (2009) 336.
[4] M. Yurechko, A. Fattah, T. Velikanova, B. Grushko, J. Alloys Compd. 329 (2001) 173.
[5] V.N. Eremenko, T.D. Shtepa, Powder Metall. 3 (111) (1972) 75.
[6] T.B. Massalski, H. Okamoto, P.R. Subramanian, L. Kacprzak, Binary Alloy Phase Diagrams, 2nd ed., ASM Intern, Metals Park, OH, 1990.
[7] J. Balun, G. Inden, Intermetallics 14 (2006) 260.
[8] T. Yamamuro, Y. Morizono, J. Honjyo, M. Nishida, Mater. Sci. Eng. 438–440 (2006) 327.
[9] V.T. Witusiewicz, A.A. Bondar, U. Hecht, S. Rex, T.Ya. Velikanova, J. Alloys Compd. 465 (2008) 64.
[10] A. Grytsiv, P. Rogl, H. Schmidt, J. Giester, J. Phase Equilib. 24 (6) (2003) 511.
[11] J.C. Schuster, M.J. Palm, J. Phase Equilib. Diffus. 27 (2006) 255.
[12] B. Grushko, T.Ya. Velikanova, Calphad 31 (2007) 217.
[13] W. Kowalski, D. Pavlyuchkov, B. Grushko, M. Surowiec, J. Alloys Compd. 496 (2010) 129.
[14] J. Braun, M. Ellner, J. Alloys Compd. 309 (2000) 118.
[15] P. Villars, L.D. Calvert, Pearsons Handbook of Crystallographic Data for Intermetallic Phases, ASM, Metals Park, OH, 1985.